Investigation of NH₄OH on Zircaloy-4 Surfaces Using Electron Emission Spectroscopy

Hye Yoon Jung and Yong-Cheol Kang*

*Department of Chemistry, Pukyong National University, Busan 608-737, Korea. *E-mail: yckang@pknu.ac.kr*
Received June 4, 2007

The interaction of ammonium hydroxide (NH_4OH) with zircaloy-4 (Zry-4) was investigated using X-ray photoelectron spectroscopy (XPS) and Auger electron spectroscopy (AES) methods. In order to study the surface chemistry of NH_4OH/Zry-4 system, the binding energies of N1s, O1s and Zr3d electrons were monitored. The N1s peak intensity was remarkably increased by following cycles of Ar^+ sputtering of NH_4OH dosed Zry-4 surface at room temperature. Because the nitrogen stayed under the subsurface region was diffused out onto the Zry-4 surface after oxygen concentration was decreased. These could be occurred after the surface oxygen was diffused into the bulk or desorbed out from the surface until Ar^+ fluence was 6.0×10^{16} Ar^+/cm^2 then the surface was relatively atomic deficient state. The O1s peak intensity was decreased by stepwise Ar^+ sputtering. After many cycles of Ar^+ sputtering, the peak intensities of Zr3d peaks did not change much but the shape of the peak clearly did change. This implies that the oxidation state of zirconium was changed during stepwise Ar^+ sputtering of NH_4OH/Zry-4. The Zr3d peak intensity of zirconium nitride (ZrN_x) increased as the intensity of N1s (from zirconium nitride) increased but the Zr3d peak intensity of zirconium oxide (ZrO_x) decreased due to the depopulation of the oxygen species on the surface region. We also observed that the peak intensity of Zr^{4+} was nearly same after Ar^+ sputtering processes but the peak intensity of metallic zirconium increased compared to that of before the sputtering process was performed.

Key Words : X-ray photoelectron spectroscopy, Auger electron spectroscopy, Zircaloy-4, Ammonium hydroxide, Oxidation state

Introduction

The alloys of zirconium were developed for use as cladding material and structural material in nuclear reactors because of their low thermal neutron cross section and the corrosion resistance.[1-8] Zr-alloys are also known to dissolve large amounts of oxygen and hydrogen.[9-14] The interactions of these species on the surface and zircaloy surfaces are considered to control the environmental degradation of the alloys.[15-17] These alloys usually cause embrittlement of the structural components in those applications.

The reprocessing of spent nuclear fuel can involve high concentrations of nitrate, ammonium, peroxide ions and other reactive species such as chloride.[18] The Zry-4 is often used to construct the containment vessel for many chemicals including the chemicals stated before in engineering applications.[19] The contact of oxygen, nitrogen and hydrogen containing species with zircaloy is common to these industrial uses of zirconium. How these species chemically react on zirconium surface is hot issue in technological progress in the nuclear and chemical engineering communities.[20]

Consequently, a number of articles deal with the behavior of H_2O, D_2O and NH_3 on the alloys of zirconium.[20-25] Although many results have been published on this subject, little is known about the surface chemistry of NH_4OH which is using for pH controlling reagent,[26] on zirconium-based materials in nuclear industry.[27]

In this paper, the Ar^+ sputtering effect on 90 L (1 L = 10^{-6} torr·s) of NH_4OH dosed Zry-4 surface by using XPS and AES was described.

Experimental Section

Surface analysis was done by XPS (VG ESCALAB 2000) and AES (Omicron 4-Grid SpectaLEED). The energy analyzer of the XPS system used in this work is a concentric hemispherical analyzer (CHA). The base pressure in the analysis chamber was maintained lower than 1×10^{-10} torr. The X-ray source, a dual-anode source, is capable of delivering achromatic Mg Kα (1253.6 eV) and Al Kα (1486.6 eV) X-rays. During all experiments, spectra were obtained applying Mg Kα X-rays. X-ray source was at the high voltage of 15 kV, beam current of 15 mA, filament current of 4.2 A, pass energy of 50 eV, dwell time of 50 ms and energy step size of 1 eV in constant analyzer energy (CAE) mode at large area XPS (LAXPS) mode. High resolution spectra were obtained at pass energy of 20 eV, energy step size of 0.05 eV and other factors were kept same as used in LAXPS mode. The details were described elsewhere.[21,22] The Zry-4 surface was cleaned by Ar^+ sputtering below room temperature with 3 kV of beam energy followed by annealing to 893 K with a heating rate of 1.0 K/s. The cleanliness of the surface was verified using retarding field AES with a 3 keV of beam energy. When the survey scan of AE spectra were performed, the energy step was 1 eV, dwell time was 100 ms, and the lock-in amplifier sensitivity was 3 mV. High resolution AE spectra were taken with 0.2 eV energy step and other factors were kept same as survey scan.

The Zry-4 sample was round shape with 6.1 mm of diameter and 2.0 mm of thickness from a sheet of Zry-4. The nominal composition of Zry-4 is 1.31 wt% Sn, 0.21 wt% Fe,

0.11 wt% Cr, 0.12 wt% O, balanced with zirconium. The Zry-4 sample was mechanically ground and polished with abrasive paper and polisher (Buehler, gamma alumina, 0.05 micron). After mechanical treatment, it was ultrasonically cleaned in acetone for 10 min. Ammonium hydroxide (99.99%, Aldrich) was stored in an equilibration flask and argon ($\geq$99.99%) was connected directly to the reactive and inert section of the gas handing system, respectively. Ammonium hydroxide was purified by a few cycles of freeze-pump-thaw method and the purity of the gas was checked by a quadrupole mass spectrometer (QMS). The sample current was 1.70 μA and the argon fluence was 4.6 $\times$ 10^{15} Ar$^+$/cm^2 per one cycle of Ar$^+$ sputtering (argon pressure: 3.7 $\times$ 10^{-8} torr). Baking of the gas line was carried out as needed to maintain the purity of the gas before introducing into the main chamber. Gas exposure was performed by backfilling the chamber through a precision leak valve. XPS experiment was performed after ammonium hydroxide exposure. Representative XPS data were deconvoluted using XPSPEAK software (ver 4.1) for data analysis.

Results and Discussion

Figure 1 shows survey scans of Auger electron spectra of Zry-4 surface before and after argon ion sputtering. Asterisk marked Auger features in the figure were assigned C(KLL, 275 eV), N(KLL, 379 eV), O(KLL, 512 eV) and Zr(MNV, 147 eV).[28] There were several Zr Auger features below 150 eV of binding energy including Zr(MNN, ~92 eV). The Zr(MNV) feature was not clear when the air exposed Zry-4 surface was contaminated with carbon and oxygen. The
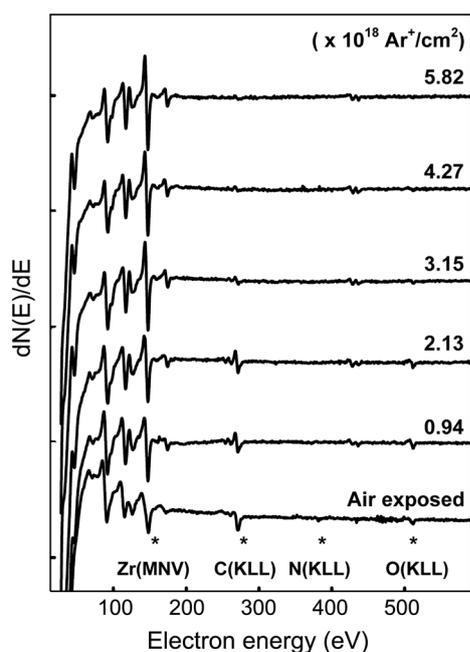

Figure 2. The survey XP spectra of NH$_4$OH/Zry-4 before and after Ar$^+$ sputtering in LAXPS mode. The numbers at the left in the figure represent integrated Ar fluence. The circled XPS features are O1s, N1s and Zr3d to emphasize.

Auger peak-to-peak heights (APPH) of the contaminating elements such as carbon, nitrogen and oxygen were decreased by following cycles of Ar$^+$ sputtering. While the APPH of Zr(MNV) was increased. Oxygen peak was always detected even sample was cleaned because of the large solid solubility of oxygen in zirconium[29] and the reactive gettering nature of the surface even under UHV conditions. The Zry-4 sample was cleaned when Ar was applied at the of fluence 3.5 $\times$ 10^{18} Ar$^+$/cm^2 to the air-exposed Zry-4 sample. XPS experiment was performed after the cleanliness of the sample was verified with AES.

The survey scan XP spectra of NH$_4$OH/Zry-4 in the range of binding energies of 0-1100.0 eV are shown in Figure 2. The bottom spectrum represents the XPS survey scan after NH$_4$OH was exposed onto Zry-4 surface. The two spectra from the top are representative survey scan after stepwise Ar$^+$ sputtering. The difference of circled XPS features in the Figure 2 of NH$_4$OH/Zry-4 system before and after Ar$^+$ sputtering should be noticed. Prominent peaks belonging to Zr3d and O1s were clearly seen at binding energies of 183.2 eV and 531.1 eV, respectively. The XPS peak intensities of C1s (286.1 eV) and N1s (397.0 eV) were also changed before and after Ar$^+$ sputtering.

The XPS peak intensity of O1s was reduced after Ar$^+$ sputtering, however Zr3d peak intensity was increased compare to that of before Ar$^+$ sputtering. Carbon was also found. It may be due to the amorphous carbon from carbon monoxide or carbon dioxide adsorption.[30] However, 0.32 $\times$ 10^{16} Ar$^+$/cm^2 bombardment was enough to clean the Zry-4 surface in terms of carbon contamination.

The representative O1s XP spectra following cycles of Ar$^+$ sputtering are stacked in Figure 3(a). The comparison of XP spectra of the O1s region before and after Ar$^+$ sputtering is shown in Figure 3(b) and 3(c), respectively. The oxygen peak may come from surface adsorption and hydroxyl ion.[29] The deconvolution of the O1s peak in Figure 3(c) revealed two components[5,31] centered at 531.1 eV and 532.8 eV those were attributed to the hydroxyl ion and O^{2-}, respectively. After stepwise Ar$^+$ sputtering, total O1s peak intensity was

Figure 1. The survey AE spectra of air exposed Zry-4 before and after stepwise Ar$^+$ sputtering. The numbers at the right in the figure represent integrated Ar fluence. The * marks indicate featured Auger peaks of NH$_4$OH/Zry-4 system.
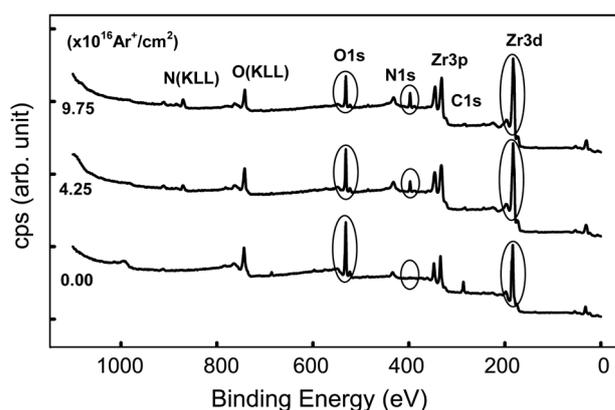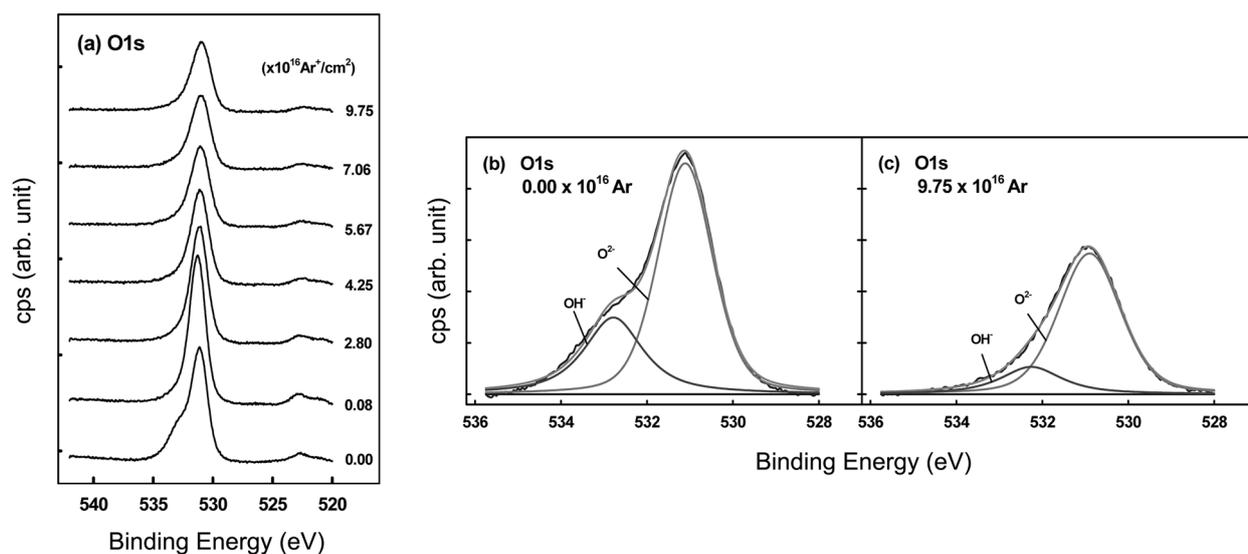
Figure 3. (a) XP spectra of the O1s region after argon ion sputtering indicates a strong reduction of O1s. Deconvoluted XP spectra of the O1s region in NH₄OH/Zry-4 (b) before and (c) after Ar$^+$ sputtering. Wiggly lines in (b) and (c) represent raw data, smooth lines overlapped with raw data are reconstructed data and bottom solid lines are background. The component centered at 531.0 eV is attributed to the hydroxyl ion and 532.8 eV is attributed to the presence of O^{2-} ions.
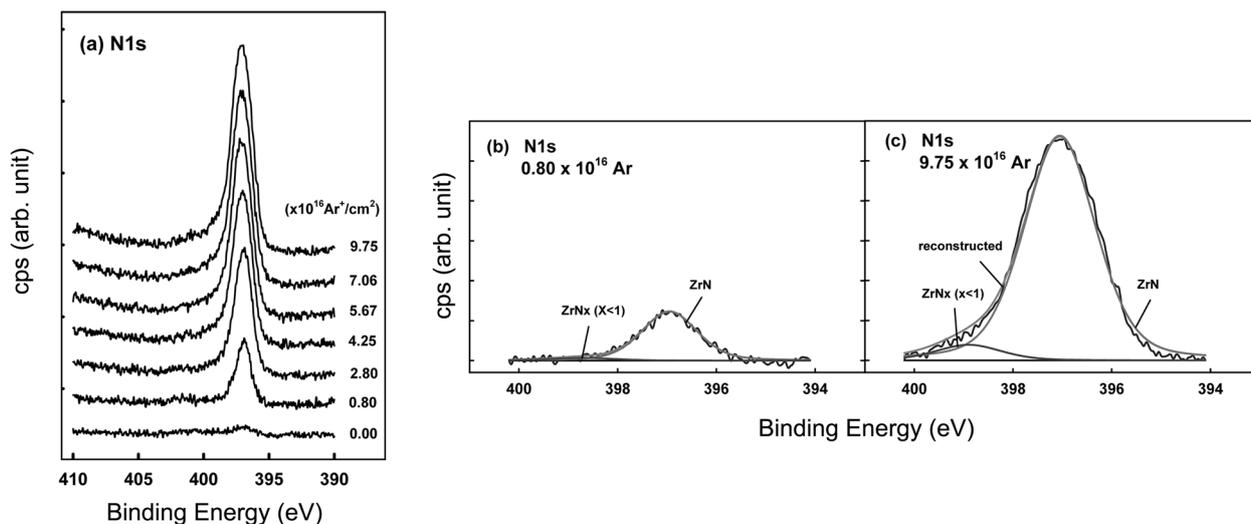

Figure 4. (a) stacked XP spectra of the N1s region after argon ion sputtering processes indicate a strong increase of N1s. Deconvoluted XP spectra of the N1s region in NH₄OH/Zry-4 (b) after 0.8 × 10^{16} Ar$^+$ fluence and (c) after 9.75 × 10^{16} Ar$^+$ fluence. Wiggly lines in (b) and (c) represent raw data, smooth lines overlapped with raw data are reconstructed data and bottom solid lines are background. N1s of ZrN is centered at 387.1 eV and N1s of ZrN$_x$ (x < 1) is centered at 398.9 eV.

decreased. This may be happened because the surface oxygen was diffused into the bulk or sputtered out during stepwise Ar$^+$ sputtering. After the concentration of oxygen near the surface region was decreased, nitrogen stayed under the surface region was diffused out to the deficient sites on the surface region caused increasing of the N1s peak intensity. Figure 4(a) presents a set of high resolution N1s XP spectra of NH₄OH/Zry-4 following cycles of Ar$^+$ sputtering. The N1s peak intensity was remarkably growing after cycles of Ar$^+$ sputtering. Yamamoto *et al.* reported that nitrogen is more stable than oxygen species on zirconium surface.[20,23,32] They reported that weakly bound oxygen

species is desorbed from the surface then nitrogen stayed under the subsurface region diffused out onto the zircaloy surface. The N1s XP spectrum showed a main component centered at 397.1 eV and a less intense peak centered at 398.9 eV after Ar$^+$ sputtering, which were attributed to ZrN and ZrN$_x$ (x < 1) shown in Figure 4(b) and 4(c).[29,33] The comparison of the data between Figure 4(b) and 4(c) revealed that the intensities of N1s peaks from ZrN and ZrN$_x$ (x < 1) increased sharply after stepwise Ar$^+$ sputtering. According to these results, we could confirmed that the subsurface region nitrogen was diffused out to the deficient sites of the Zry-4 surface. The propensity of peak intensities
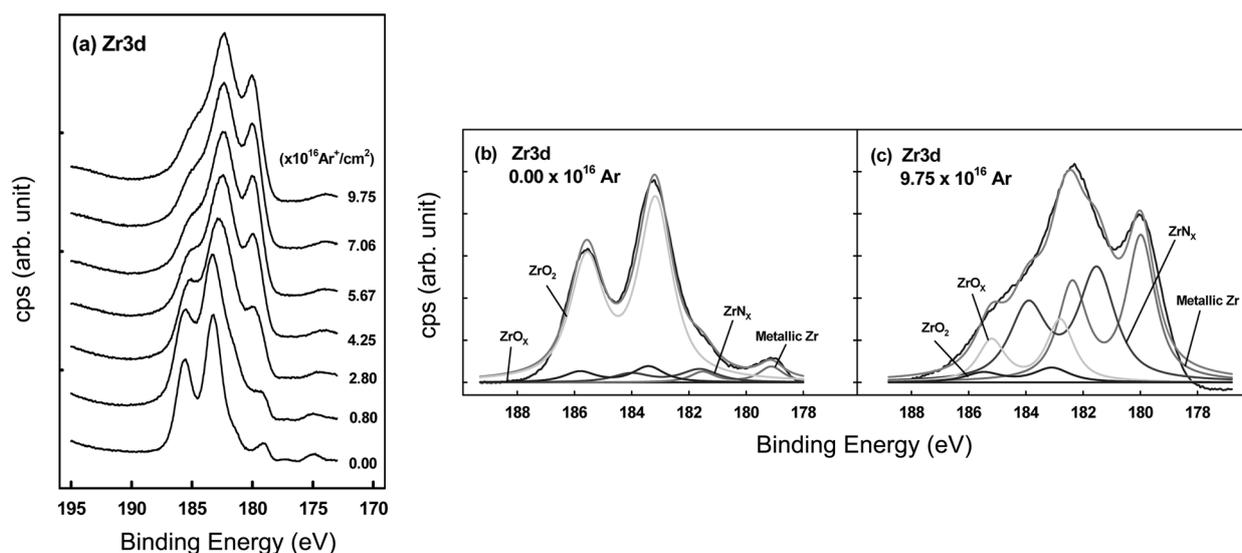
Figure 5. (a) XP spectra of the Zr3d region following cycles of Ar^+ sputtering. XP spectra of the Zr3d region in NH_4OH/Zry-4 (b) before and (c) after Ar^+ sputtering. Wiggly lines in (b) and (c) represent raw data, smooth lines overlapped with raw data are reconstructed data and bottom solid lines are background. Zr3d of metallic zirconium is centered at 179.1 eV, Zr3d of ZrN_X is centered at 181.6 eV, Zr3d of ZrO_X is centered at 398.9 eV and Zr3d of zirconia is centered at 183.4 eV.

of N1s and O1s by following cycles of Ar^+ sputtering is plotted in Figure 6(a) and 6(b), respectively. Our results were well supported by previous results of Yamamoto's work. When the sample surface was clean in terms of carbon contamination by cycles of Ar^+ sputtering, oxygen intensity of the surface was almost stayed same after Ar fluence of 6.0 $\times 10^{16}$ Ar^+/cm^2 was applied as shown in Figure 6(b). This phenomenon is common to zirconium system as oxygen solid solution state.[34]

The comparison of XP spectra of the Zr3d region before and after Ar^+ sputtering is shown in Figure 5(b) and 5(c). Zr3d XP spectra consist of one main set of doublet *i.e.* $Zr3d_{3/2}$ and $Zr3d_{5/2}$ peaks. After stepwise Ar^+ sputtering, the intensity of Zr3d XP spectra did not change much but the shape of the peak clearly changed as shown in Figure 5(a). Before Ar^+ sputtering, the Zr3d XP spectra could be decon-

voluted into four components, *i.e.* metallic Zr (179.1 eV), zirconium nitride (ZrN_x, 181.6 eV),[5] zirconium oxide (ZrO_x, 183.2 eV) and Zr^{4+} (zirconia, 183.4 eV). The zirconium oxynitride formation was excluded in this system. The Zr3d peak intensity of zirconium nitride (ZrN_x) increased following Ar^+ sputtering cycles. However, after stepwise Ar^+ sputtering, the peak intensity of zirconium oxide (ZrO_x) decreased. This was well matched with the results of oxygen intensity was decreased and nitrogen intensity was increased by stepwise Ar^+ sputtering.

The Zr^{4+} intensity was nearly same as before and after Ar^+ sputtering process but the peak intensity of metallic zirconium increased compared to that of before the sputtering process. The intensity of ZrN_x was increased following cycles of Ar^+ sputtering because the subsurface nitrogen was diffused out onto the Zry-4 deficient sites. However the
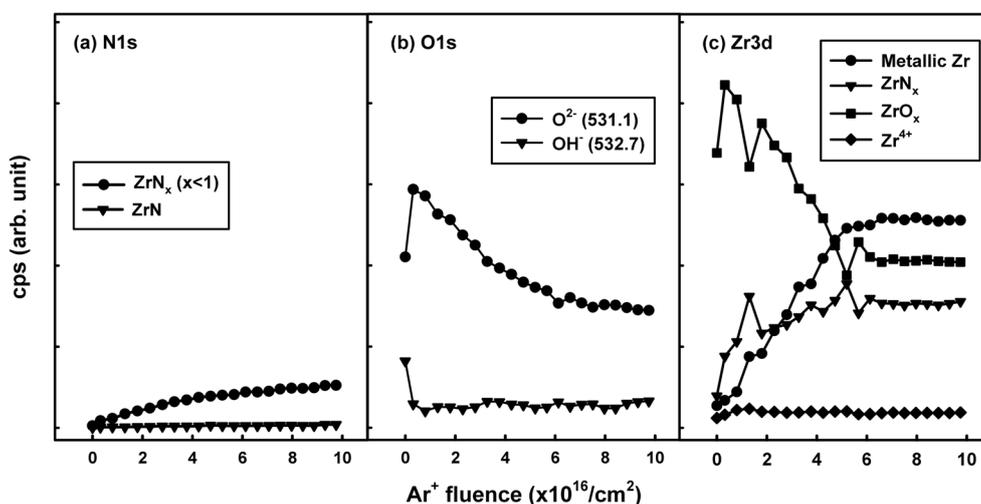

Figure 6. The area of deconvoluted XPS peaks of NH_4OH/Zry-4 surface as a function of argon fluence N1s, (b) O1s and (c) Zr3d.

ZrO_x was deceased after stepwise Ar^+ sputtering according to the total O1s peak intensity was deceased shown in Figure 6(c).

Conclusions

The AES experiment was performed to check the cleanliness of Zry-4 surface. The APPHs of C(KLL), N(KLL) and O(KLL) were decreased while that of Zr(MNV) was increased by following stepwise Ar^+ sputtering. Before NH₄OH dosed on Zry-4 surface, Ar^+ fluence of 3.5×10^{18} Ar^+/cm^2 was enough to clean the Zry-4 surface in terms of carbon contamination. The interaction of NH₄OH with Zry-4 surface was investigated using XPS methods after cleanliness Zry-4 was verified. The results showed that the changes of XPS intensities of O1s, N1s and Zr3d by stepwise Ar^+ sputtering. During the stepwise Ar^+ sputtering, oxygen peak intensity was decreased while nitrogen peak intensity was increased. This could be happened because the weakly bound oxygen was diffused into the bulk or desorbed out from the surface then the nitrogen stayed subsurface region diffused out to the deficient sites on the surface region. This conversion of oxygen and nitrogen intensities caused increasing of zirconium nitride intensity and decreasing of zirconium oxide intensity. After the Ar fluence of 6.0×10^{16} Ar^+/cm^2 was applied to the NH₄OH/Zry-4 system, the peak intensities of O1s, N1s and Zr3d were stayed same. This implies that the system was recovered to clean limit.

References

1. Ahmad, M.; Akhter, J. I.; Ali, G.; Akhtar, M.; Choudhry, M. A. *J. Alloy Compd.* **2006**, *426*, 176.
2. Meyer, G.; Kobrinsky, M.; Abriata, J. P.; Bolcich, J. C. *J. Nucl. Mater.* **1996**, *229*, 48.
3. Hsu, H.-H. *J. Alloy Compd.* **2006**, *426*, 256.
4. Lim, B. H.; Hong, H. S.; Lee, K. S. *J. Alloy Compd.* **2003**, *312*, 134.
5. Wiame, H.; Centeno, M.-A.; Picard, S.; Bastians, P.; Grange, P. *J. Eur. Ceram. Soc.* **1998**, *18*, 1293.
6. Peng, D. Q.; Bai, X. D.; Pan, F.; Sun, H.; Chen, B. S. *Appl. Surf. Sci.* **2005**, *252*, 1793.
7. Inoue, M.; Yamashita, M.; Suganuma, K.; Nunogaki, M. *J. Nucl. Sci. Technol.* **2001**, *38*, 980.
8. Chemelle, P.; Knorr, D. B.; Van Der Sande, J. B.; Pelloux, R. M. *J. Nucl. Mater.* **1983**, *113*, 58.
9. Fromm, E.; Jehn, H. *Bull. Alloy Phase Diagrams.* **1984**, *5*(3), 323.
10. Konev, V. N.; Nadolskii, A. L.; Minyacheva, L. A. *Oxidation Metals* **1997**, *47*(3/4), 237.
11. Yamanaka, S.; Miyake, M.; Katsura, M. *J. Nucl. Mater.* **1997**, *247*, 315.
12. Galan, P. P.; Sanz, L.; Rueda, J. M. *Surf. Interface. Anal.* **1990**, *16*(1-12), 535.
13. Choo, K. N.; Kim, Y. S. *J. Nucl. Mater.* **2001**, *297*, 52.
14. Zhang, C.-S.; Norton, P. R. *J. Nucl. Mater.* **2002**, *300*, 7.
15. Roustila, A.; Chêne, J.; Séverac, C. *J. Alloy Compd.* **2003**, *356*, 330.
16. Cox, B. *J. Alloy Compd.* **1997**, *256*, 244.
17. Khatamian, D. *J. Alloy Compd.* **1997**, *253*, 471.
18. Bellanger, G.; Rameau, J. J. *J. Mater. Sci.* **2000**, *35*, 1759.
19. Yau, T. L.; Paul, B. O.; Henson, R. H. *Chem. Process* **1999**, *62*, 70.
20. Kang, Y. C.; Ramsier, R. D. *Vacuum* **2002**, *64*, 113.
21. Kwon, J. H.; Youn, S. W.; Kang, Y. C. *Bull. Korean Chem. Soc.* **2006**, *27*, 11.
22. Oh, K. S.; Kang, Y. C. *Bull. Korean Chem. Soc.* **2007**, *28*, 1341.
23. Stojilovic, N.; Kang, Y. C.; Ramsier, R. D. *Surf. Interface Anal.* **2002**, *33*, 945.
24. Hong, H. S.; Kim, S. J.; Lee, K. S. *J. Nucl. Mater.* **1999**, *273*, 177.
25. Stojilovic, N.; Ramsier, R. D. *Appl. Surf. Sci.* **2006**, *252*, 5839.
26. Stojilovic, N.; Bender, E. T.; Ramsier, R. D. *J. Nucl. Mater.* **2006**, *348*, 79.
27. Cohen, P. *Water Coolant Technology of Power Reactors*; American Nuclear Society: USA, 1980.
28. Kang, Y. C.; Ramsier, R. D. *J. Nucl. Mater.* **2002**, *125*, 303.
29. (a) Rizzo, A.; Signore, M. A.; Mirenghi, L.; Serra, E. *Thin Solid Films* **2006**, *515*, 1307. (b) Rizzo, A.; Signore, M. A.; Mirenghi, L.; Dimaio, D. *Thin Solid Films* **2006**, *515*, 1486.
30. Gu, Y.; Guo, F.; Qian, Y.; Zheng, H.; Yang, Z. *Mater. Lett.* **2003**, *57*, 1679.
31. Zhu, X. L.; Liu, S. B.; Man, B. Y.; Xie, C. Q.; Chen, D. P.; Wang, D. Q.; Ye, T. C.; Liu, M. *Appl. Surf. Sci.* **2007**, *253*, 3122.
32. Yamamoto, M.; Kurahashi, M.; Chan, C. T.; Ho, K. M.; Naito, S. *Surf. Sci.* **1997**, *387*, 300.
33. Benia, H. M.; Guemmaz, M.; Schmerber, G.; Mosser, A.; Parlebas, J. C. *Appl. Surf. Sci.* **2003**, *211*, 146.
34. Tanabe, T.; Tomita, M. *Surf. Sci.* **1989**, *222*, 84.